Controlling the Shape and Flexibility of Arylamides: A Combined ab Initio, ab Initio Molecular Dynamics, and Classical Molecular Dynamics Study†

Vojislava Pophristic,*,‡ Satyavani Vemparala,§ Ivaylo Ivanov,|| Zhiwei Liu,‡ Michael L. Klein,§ and William F. DeGrado⊥

Department of Chemistry and Biochemistry, University of the Sciences in Philadelphia, Philadelphia, Pennsylvania 19104, Departments of Chemistry and Biophysics and Medical School, University of Pennsylvania, Philadelphia, Pennsylvania 19104, and Department of Chemistry and Biochemistry, University of California—San Diego, La Jolla, California 92093

Received: August 3, 2005; In Final Form: December 19, 2005

Using quantum chemistry plus ab initio molecular dynamics and classical molecular dynamics methods, we address the relationship between molecular conformation and the biomedical function of arylamide polymers. Specifically, we have developed new torsional parameters for a class of these polymers and applied them in a study of the interaction between a representative arylamide and one of its biomedical targets, the anticoagulant drug heparin. Our main finding is that the torsional barrier of a $C_{aromatic}-C_{carbonyl}$ bond increases significantly upon addition of an *o*-$OCH_2CH_2NH_3^+$ substituent on the benzene ring. Our molecular dynamics studies that are based on the original general AMBER force field (GAFF) and GAFF modified to include our newly developed torsional parameters show that the binding mechanism between the arylamide and heparin is very sensitive to the choice of torsional potentials. Ab initio molecular dynamics simulation of the arylamide independently confirms the degree of flexibility we obtain by classical molecular dynamics when newly developed torsional potentials are used.

I. Introduction

In the past decade, there has been an increasing interest in synthetic polymers that mimic naturally occurring polypeptides with certain biochemical roles.[1−6] Arylamide polymers, consisting of aromatic rings connected by amide bonds, take a special place among the biomimetic polymers because of the diverse biomedical functions they have been designed to have, as well as the easiness and low cost of their synthesis. For example, arylamide polymers with amphiphilic structure have been successfully created to mimic naturally occurring antimicrobial peptides such as magainin (Figure 1a).[2] Recently, an arylamide polymer (Figure 1b) with high potency as a heparin antidote has been designed.[7] Some related compounds attract attention for quite a different reason: many naturally occurring aromatic amines are known or suspected carcinogens.[8] Thus, different arylamide/arylamine forms have been the focus of diverse research efforts ranging from computational chemistry and organic synthesis to biomedical applications.[1,9−14] To fully utilize the arylamide properties for biomedical applications, increase their effectiveness and specificity, and optimize the design efforts, one needs to understand the interactions between the arylamides and their biochemical targets at the molecular level. Computational chemistry has been shown to contribute greatly to such an understanding because of the level of detail it provides. In this work, we combine quantum chemical and molecular dynamics analyses to provide valuable insight into the conformation and properties of a class of arylamide polymers.

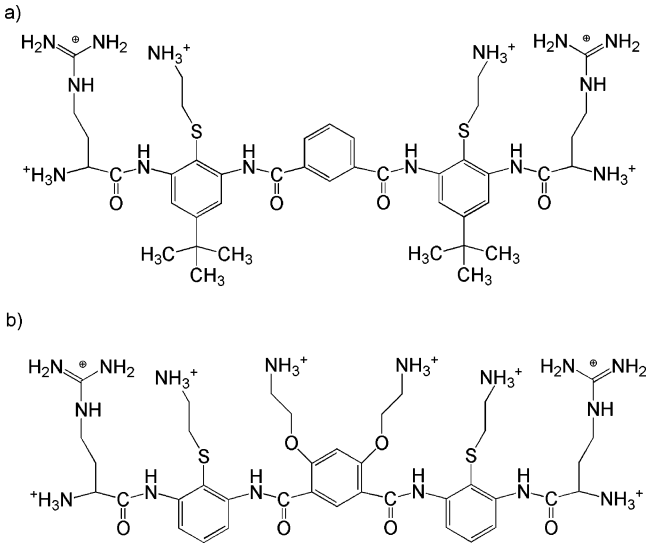

Figure 1. Two functional forms of arylamide polymers: (a) arylamide with antimicrobial activity (compound **1**), (b) arylamide with heparin-antidote activity (compound **2**).

A common structural feature of the arylamide polymers of interest is a backbone consisting of benzene rings connected by peptide bonds (Figure 1). The differences between the two arylamide compounds arise mainly from the nature of the side chains attached to the benzene rings. Conformation of the molecule, dictated primarily by internal rotations of the backbone but also influenced by the nature of the side chains, determines both the roles that synthetic arylamides play as

† Part of the special issue "Michael L. Klein Festschrift".

* Corresponding author. E-mail: v.pophri@usip.edu.
‡ University of the Sciences in Philadelphia.
§ Department of Chemistry, University of Pennsylvania.
|| University of California—San Diego.
⊥ Department of Biophysics and Medical School, University of Pennsylvania.

10.1021/jp054306+ CCC: $33.50
Published on Web 02/08/2006

biomedical agents and their effectiveness. Thus, information about the shape of a molecule in solution and relative orientations of side chains is usually of critical importance for the design efforts. The aim of our study is to show how backbone flexibility of an arylamide polymer can be controlled and in turn how it influences the polymer's biochemical function.

Our focus has been on two forms of arylamide polymers: highly positively charged arylamides acting as heparin antidotes[7] and amphiphilic arylamides with antimicrobial activity (Figure 1).[2] Both applications are of great significance from a biomedical standpoint: an effective heparin antidote would reduce the risk of excessive bleeding in patients under heparin treatment (the category which includes all patients undergoing surgeries where an antithorbotic agent is required, such as bypass surgeries), and antimicrobial arylamides could substantially reduce the health problems (including mortality) associated with healthcare acquired infections. Antimicrobial and heparin-antidote arylamide polymers have similar chemical structures (parts a and b of Figure 1), with important differences in polarity and location of the side chains. The antimicrobial form (Figure 1a, **1**) has a molecular formula with charged groups on one face of the molecule and hydrophobic groups on the other, whereas the heparin-antidote form (Figure 1b, **2**) has a high positive charge and lacks hydrophobic groups. It is believed that naturally occurring antimicrobial peptides derive their function from the common structural feature of amphiphilicity (spatial separation of hydrophobic and hydrophilic groups within a molecule).[6] Although at a first glance **1** appears amphipathic, this feature depends heavily on the conformation the molecule will assume in solution and at lipid bilayer interfaces. Its shape will be determined by the flexibility of the backbone, that is, torsional motions around the bonds that connect benzene rings. Similarly, backbone torsions will influence the interaction mode of **2** with its biological target, heparin, due to the fact that the arylamide potency will be increased by maximizing the number of contacts between the positively charged arylamide side chains and negatively charged heparin groups. We first focus on the torsional barriers of bonds comprising the backbone and how they depend on the intramolecular environment of the particular bond undergoing internal rotation. On the basis of improved torsional parameters, we then present a molecular dynamics study of the flexibility of the arylamide backbone in aqueous solution. Our results show that it is essential to take into account intramolecular environment when dealing with this class of molecules, in order to obtain an accurate view of the mechanism of their biochemical functions. This is especially true when molecular flexibility (or rigidity) plays a role in such a mechanism.

The article is organized as follows: we briefly describe the methods and conditions used in ab initio, ab initio molecular dynamics, and classical molecular dynamics simulations (section II). We then discuss the torsional potentials of the small model compounds obtained from ab initio calculations (section III.A), how the molecular dynamics description of flexibility and shape of the arylamide in question changes upon applying different torsional parameters (section III.B), how these results agree with the ab initio molecular dynamics data of a reduced form of the heparin-antidote arylamide (section III.C), and finally how torsional parameters influence arylamide/heparin interaction (section III.D). We conclude (sections IV and V) by comparing the results obtained from parametrized and ab initio simulations and by discussing the relationship between the torsional potentials and the conformational flexibility of the arylamide in solution.

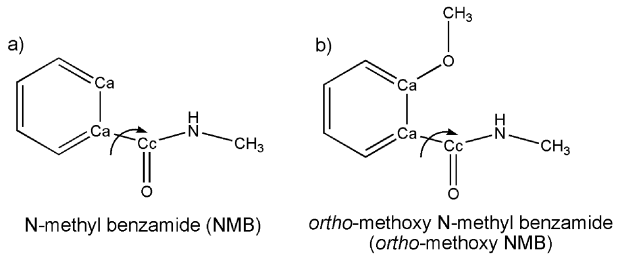

Figure 2. Equilibrium structures of *N*-methyl benzamide (a) and *o*-methoxy *N*-methyl benzamide (b). Arrows illustrate torsions modeled in this work. C_a refers to aromatic carbon atoms, and C_c refers to carbonyl carbon atoms.

II. Methodology

The study was conducted using methods from three computational chemistry areas: quantum chemistry, ab initio molecular dynamics, and classical (all-atom) molecular dynamics. Torsional potentials around the backbone bonds were obtained by quantum chemistry methods applied to model compounds derived from the formula of **2**. Dependence of the backbone flexibility on the intramolecular structure of the molecule was investigated using ab initio and classical molecular dynamics simulations in gas phase and aqueous solution.

Torsional Potentials. Torsional energy profiles were calculated for a number of model compounds that capture the essential structural features of **2**, such as steric hindrance between S and O atoms and hydrogen-bonding between S and H (of the NH group) and between H (of the benzene ring) and O (of the C═O group) atoms (Figure 1). Here we focus on the torsions around the $C_{aromatic}-C_{carbonyl}$ (C_a-C_c) bond of *N*-methylbenzamide (NMB), which has the greatest influence on the rigidity of the arylamide backbone (Figures 1b and 2a), and its derivative, *o*-methoxy *N*-methylbenzamide (*o*-methoxy NMB) (Figure 2b).[15] The equilibrium geometries were obtained by full optimization at HF, MP2, BLYP, and B3LYP levels, using a series of basis sets (Table 1, discussed in section III.A). Initially, torsional energy profiles were obtained by scanning the torsional potential surface in 10° increments at B3LYP/6-31G(d) and B3LYP/6-311G(d,p) levels. At each scan point, all internal coordinates except the torsional angle driving the scan were optimized. Torsional barriers were also calculated at the other levels used for the equilibrium conformers by constraining the torsional angle defining the maxima (Table 2, see also Tables 1S and 2S in the Supporting Information). The true transition states were obtained by refining the maxima of the scan using transition state optimizations at selected computational levels. To ensure that the optimized geometries correspond to minima or transition states, harmonic frequencies were calculated, and in the case of transition states, vibrational modes corresponding to the imaginary frequencies were determined to be the torsions in question. All quantum chemical calculations were carried out by Gaussian03 [16] and NWChem software.[17,18]

Ab Initio Molecular Dynamics. The ab initio molecular dynamics (AIMD)[19] part of the study was conducted using CPMD software.[20] A 9 ps AIMD simulation of a reduced arylamide structure was performed using the HCTH density functional[21] and ultrasoft pseudopotentials.[22,23] The electronic wave functions were described by a plane wave basis with a 25 Ry cutoff. The simulation was performed in the gas phase, in a periodically repeating box of dimensions $22 \times 10 \times 26$ Å^3. The system was equilibrated using a Nose−Hoover chain thermostat (of chain length 4, with a frequency of 1000 cm^{-1}) at 300 K.[24−27] We employed a time step of 0.14484 fs and a

TABLE 1: Geometries of *o*-Methoxy NMB and NMB Compounds at Representative Computational Levels

	NMB				*o*-methoxy NMB			
	HF 6-311 G(3df,2p)	MP2 6-311 G(2d,p)	B3LYP 6-311 G(d,p)	B3LYP 6-311 G(3df,2p)	HF 6-311 G(3df,2p)	MP2 6-311 G(2d,p)	B3LYP 6-311 G(d,p)	B3LYP 6-311 G(3df,2p)
bond lengths (Å)								
C_a-C_c	1.502	1.499	1.506	1.503	1.513	1.513	1.516	1.513
C_c-O	1.194	1.226	1.222	1.219	1.199	1.230	1.225	1.222
C_c-N	1.352	1.368	1.368	1.364	1.340	1.352	1.359	1.354
C_a-O					1.347	1.376	1.373	1.368
angles (deg)								
$C_aC_aC_c$	123.1	122.8	123.5	123.5	127.1	127.0	127.5	127.2
C_aC_cN	116.6	115.5	115.8	116.3	119.1	117.9	117.6	118.4
C_aC_cO	121.3	122.1	121.5	121.7	119.7	120.6	119.9	120.4
dihedral angles (deg)								
$OC_aC_aC_c$					0.0	0.0	0.0	0.0
$C_aC_aC_cO$	25.35	25.3	22.1	22.8	180.0	179.7	180.0	180.0
$C_aC_aC_cN$	25.0	24.2	23.8	22.3	0.0	0.3	0.0	0.0

TABLE 2: Energies of the NMB and *o*-Methoxy NMB Conformers Corresponding to the Maxima of the Torsional Potential Curve Relative to the Equilibrium Conformer Energies at Various Computational Levels (kcal/mol)

	NMB		*o*-methoxy NMB		
	90° conformer	TS conformer	100° conformer	180° conformer	TS conformer[a]
HF/6-311G(2d,p)	3.85	3.83	3.91	8.26	8.90
HF/6-311G(3df,2p)	3.69		3.79	8.31	
MP2/6-31G(2d,p)	3.93		4.90	8.26	9.00
MP2/6-311G(2d,p)	3.52	3.52	4.34	8.14	
B3LYP/6-311G(d,p)	3.68	3.68	5.55	9.16	9.43
B3LYP/6-311G(2d,p)	3.61	3.61	5.04	8.34	8.70
B3LYP/6-311G(3df,2p)	3.40	3.41	4.89	8.24	

[a] Refers to the transition state in vicinity of the 180° $C_a-C_a-C_c-N$ dihedral angle.

fictitious mass for the electronic degrees of freedom of $\mu = 600$ au.

Molecular Dynamics Simulations. All-atom molecular dynamics (MD) was used to analyze the behavior of **2** in aqueous solution, alone, and in the presence of heparin. Two sets of parameters for arylamide were used; one derived from the general AMBER force field (GAFF)[28] and another one derived from GAFF with modified torsional parameters to reflect the specific arylamide intramolecular environment as obtained by calculations described above. Comparison of simulations with the two force fields allows the effect of backbone rigidity on the conformation of the molecule and its biomedical function to be estimated. The arylamide structure was constructed according to Figure 1b and initially had three benzene rings and all amide links in one plane. Arylamide charges were assigned in a manner consistent with the AM1-BCC model.[29,30] The simulated heparin−pentasaccharide structure was extracted from the Protein Data Bank (PDB) structure of heparin−antithrombin III complex (PDB ID code 1E03). Parameters for heparin were developed partly by analogy with the existing GLYCAM[31]/AMBER[32,33] and OSO_3^- parameters[34] and partly from semiempirical (MOPAC) calculations. In the case of arylamide in water (no heparin present), the simulation time step was 1 fs with GAFF and 0.5 fs with modified GAFF. The simulation box size was $58 \times 47 \times 65$ Å^3, with ~4500 TIP3P[35] water molecules and 8 Cl^- ions to balance the charge. The arylamide/heparin/water system was studied using conventional MD as well as replica-exchange method (REM, also referred to as parallel tempering).[36] The following parameters were used for setting up the conventional MD. The step size was 1 fs with GAFF and 1.5 fs with modified GAFF. The corresponding simulation box size was $60 \times 57 \times 65$ Å^3, with ~5500 TIP3P water molecules and 3 Na^+ ions to balance the charge. Both the arylamide/water and arylamide/heparin/water (conventional MD) systems were run using the NAMD simulation package.[37] The systems were equilibrated for 2−3 ns in the NPT ensemble, at a temperature of 300 K and a pressure of 1 atm. We employed periodic boundary conditions and the particle mesh Ewald (PME) method for calculating long-range electrostatic forces. The analysis (see below) was performed based on production run trajectories (3−5 ns for arylamide/water system; 5−7 ns for the arylamide/heparin/water system).

A replica-exchange method[36] was used in the case of the arylamide/heparin/water system to provide sufficient sampling of the conformational space. Two sets of REM simulations were carried out, one with the original GAFF and another one with the modified GAFF, both using AMBER8.[38] Initially, eight configurations were extracted at different time steps from a conventional MD simulation using original and modified GAFF (four from each). Each of the eight arylamide/heparin/Na^+ conformations was placed into a simulation box of $57 \times 57 \times 57$ Å^3 size, and 5740 water molecules were added. Several short REM trial simulations (using modified GAFF) were performed to find the optimal temperature distributions. We found that for an exchange ratio of 30−50% to be obtained, a temperature series of 290.0, 292.0, ..., 401.9, 404.7, ..., 549.5, and 553.3 K with 96 different temperatures is needed. A total of 96 different conformations were taken from the conformations saved in the trial runs. Each of the 96 replicas was equilibrated for 200 ps in the NPT ensemble (using modified GAFF), at a temperature of 300 K and a pressure of 1 atm. The final size of the simulation box was $\sim 56 \times 56 \times 56$ Å^3. The equilibrated structures were used as starting structures for the production REM simulations (NVT ensembles with 96 different temperatures) with both original and modified GAFF. A time step of 1 fs, with a RESPA time step of 4 fs, and SHAKE algorithm to constrain the O−H bond in water molecules, along with PME in calculating long-range electrostatic forces in the periodic systems, were employed. A 2 ps interval between two attempts of exchange between adjacent temperatures was used. The time interval of

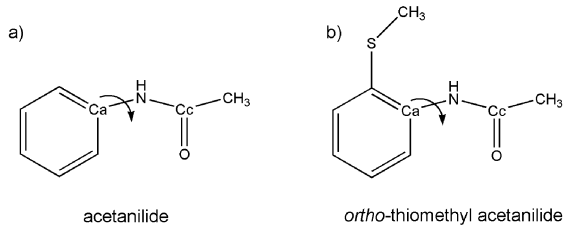

Figure 3. Equilibrium structures of acetanilide (a) and *o*-thiomethyl acetanilide (b). Arrows illustrate torsions discussed in this work. C_a refers to aromatic carbon atoms, and C_c refers to carbonyl carbon atoms.

2 ps was much larger than the coupling time of the heat bath (0.2 ps) so that the system was roughly equilibrated before each next exchange. Each replica was run for 4 ns, yielding a total sampling time of 384 ns for original or modified GAFF. Conformations were saved every 1 ps. The presented analyses are based on conformations saved at 300 K.

III. Results

The shape of an arylamide polymer is controlled primarily by the conformation of its backbone, which is, in turn, determined by internal rotations around three bonds: C_a-C_c, C_c-N, and $N-C_a$ (Figures 1, 2, and 3). The peptide (C_c-N) bond is known to be rigid with respect to torsion because of its partial double bond character. Thus, the other two degrees of freedom are the primary determinants of the flexibility of arylamide oligomers. The torsional barrier for acetanilide (featuring the C_a-N torsion, Figure 3a) has been calculated to be 4 kcal/mol[10,11] and to increase upon addition of a hydrogen-bond-accepting substituent in the ortho position (Figure 3b). Such a finding implies that similar substitutions in the arylamide polymer would result in an increased rigidity of the backbone. This influence, however, has not been investigated beyond the reduced model compounds, such as *o*-methylthioacetanilide. We first analyzed the degree of flexibility control that can be achieved by structural alterations in the vicinity of the C_a-C_c bond; we then apply lessons learned from quantum mechanical studies to the full system, that is, the arylamide oligomer shown in Figure 1b, by performing and systematically analyzing MD and AIMD simulations.

III.A. Torsional Potentials of NMB and *ortho*-Methoxy NMB. Several studies on the NMB equilibrium conformer have been published, analyzing its geometry at various levels of theory.[39,40] However, experimental data for either NMB or *o*-methoxy NMB are not available. We performed a careful convergence study of equilibrium geometries of these compounds, using full optimization at HF, MP2, BLYP, and B3LYP levels with basis sets ranging from 6-3G(d) to 6-311G(3df,2p). Table 1 shows that B3LYP/6-311G(d,p) geometrical parameters of NMB are in close agreement with the HF and MP2 values, with the bond lengths and angles either slightly higher or similar to HF and MP2 values and dihedral angle values somewhat lower. Addition of the polarization basis set functions does not significantly change the geometrical parameters at any of the attempted levels. Our B3LYP/6-311G(d,p) results agree also with the previously published work of Vargas et al. (MP2/DZP and BLYP/DZVP2 levels).[40] The only exception is the $C_a-C_a-C_c-O$ dihedral angle, which in our case is 25° at the HF and MP2 levels, 24° at the BLYP level, and 23° at the B3LYP level, as opposed to ~28° obtained in ref 40. However, our equilibrium $C_a-C_a-C_c-N$ angle is close to the experimental average value derived by Vargas et al.[40] from related compounds with available X-ray structures in the Cambridge Structural Database.[41] Our value also favorably compares to the equivalent dihedral angle obtained for benzamide at the B3LYP/6-31+G-(d,p) level,[42] indicating that diffuse functions are not critical for a proper description of NMB geometry.

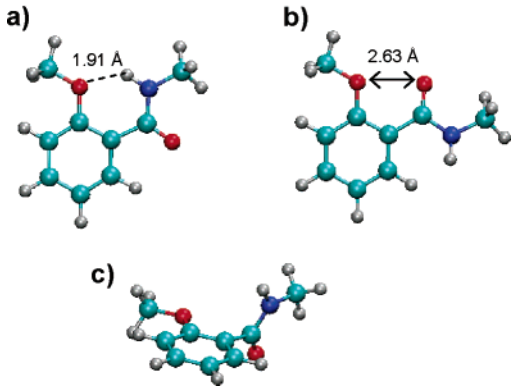

Figure 4. Equilibrium (a), 180° (b), and 90° (c) conformers of *o*-methoxy NMB: carbon, blue; oxygen, red; nitrogen, dark blue; hydrogen, silver. Upon 180° internal rotation around the C_a-C_c bond, the hydrogen bond between the H (NH) and O (C_a-O) atoms is broken, and two oxygen atoms become close to each other. Both events destabilize the 180° conformer with respect to the equilibrium one.

Results of the convergence study in the case of *o*-methoxy NMB geometry are similar. The B3LYP/6-311G(d,p) optimized geometry is close to the highest basis set MP2 optimization performed and is not influenced much by the basis set increase at the B3LYP level (Table 1). We therefore adopt the B3LYP/6-311G(d,p) level for the geometry optimizations of conformers that correspond to different $C_a-C_a-C_a-N$ torsional angles needed for obtaining a torsional energy profile.

The equilibrium geometry of NMB (Table 1) is characterized by pronounced nonplanarity between the aromatic ring and the amide group (the amide group is tilted out of plane by ~20°). Addition of an OCH_3 group in the ortho position however removes this feature, making the *o*-methoxy NMB form planar (Table 1, Figure 4). In the optimized *o*-methoxy NMB structure, the C═O bond points away from the ortho substituent, whereas the NH group is directed toward it (Figure 4). The molecule thus avoids steric crowding and achieves optimal positioning of the NH group for hydrogen-bonding to the ortho substituent. Because of the bulkiness of the two substituents, the $C_a-C_a-C_c$ angle opens up relative to NMB. The planar arrangement and orientation of the amide group brings the oxygen of the OCH_3 group and the hydrogen of the amide NH group to a distance of 1.91 Å, suitable for a hydrogen bond. The angle between the N, H, and O (of the OCH_3 group) atoms is 133.3°. This arrangement is closer to the ideal (linear) hydrogen bond than what was found for either *o*-OCH_3 or *o*-SCH_3 acetanilide (108° and 117°, respectively),[10] implying a stronger hydrogen bond in the case of *o*-OCH_3 NMB.[43]

In this work, we focus on internal rotation around the C_a-C_c bond. To derive torsional energy potentials for NMB and *o*-methoxy NMB, we scanned the potential surface at B3LYP/6-311G(d) and B3LYP/6-311G(d,p) levels, in $C_a-C_a-C_c-N$ dihedral angle increments of 10°, and obtained converging torsional barrier shapes for each molecule (Figure 5). Transition state optimizations yielded dihedral angles of the maxima within 1−2° of the ones obtained by the torsional potential surface scan. As expected, NMB has a simple, 2-fold periodic torsional potential, with a maximum at 90° (the exact position of the transition state (TS) is 91.1°), corresponding to the amide group perpendicular to the benzene ring. On the other hand, *o*-methoxy NMB has two maxima (Figures 4 and 5). One maximum is at

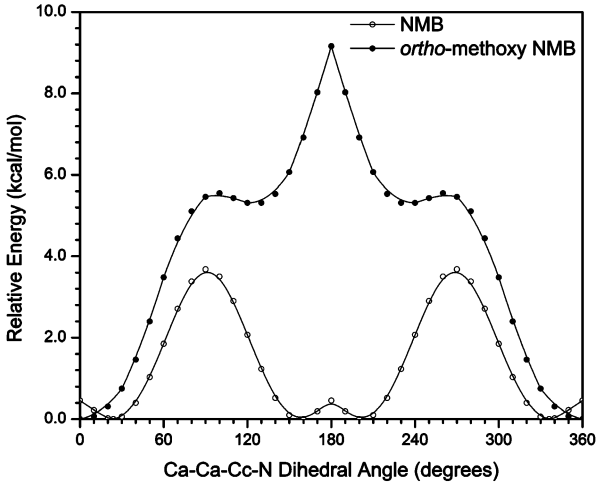

Figure 5. Potential energy profiles for torsion around the C_a-C_c bond (see Figure 2) in NMB and *o*-methoxy NMB, obtained by scanning the torsional potential surface in increments of 10° for the $C_a-C_a-C_c-N$ dihedral angle (B3LYP/6-311G(d, p) profiles shown). The original GAFF torsional profiles (not shown) for both NMB and *o*-methoxy NMB are of a cosine form ($E \propto 1 + \cos(n\phi - \text{phase})$, where n is periodicity and ϕ is the torsional angle), similarly shaped to the ab initio NMB profile but with a barrier value of ~29 kcal/mol.

~100° (TS at 98.8°). This is somewhat larger than the 90° angle in the transition state of the NMB, to accommodate the bulky ortho substituent (Figure 4c). The other one is a much higher maximum at 180°, corresponding to the conformer in which the oxygen of the carbonyl group points toward the oxygen of the ortho methoxy substituent (Figure 4b).

The calculated NMB barrier ranges from 3.5 to 3.9 kcal/mol at HF and MP2 levels and from 3.4 to 3.6 kcal/mol at the B3LYP level (Table 2). It is somewhat higher than the one obtained by Vargas et al.[40,44] In the case of *o*-methoxy NMB, Table 2 shows that the 100° barrier ranges from 3.9 to 5.6 kcal/mol and that the 180° one ranges from 8 to 9 kcal/mol. Overall, for both molecules, there is a decreasing trend in the barrier height upon a basis set increase. The transition state barriers (Table 2) are very close to the corresponding 90°, 100°, and 180° barriers obtained from the energy calculations of the conformers with geometries optimized at these (fixed) angles. The calculated NMB torsional barrier is in the vicinity of the experimentally derived barrier for the structurally closest compound featuring the C_a-C_c torsion which has such data available: the acetophenone torsional barrier has been determined from far-infrared spectra to be 3.2 kcal/mol[45] (although there are obviously large differences in molecular structure between an arylamide and an aryl ketone).

The NMB barrier can be rationalized by the increased repulsion in the 90° conformer due to the proximity of the electron clouds of the carbonyl group and the π system of the benzene ring (Figure 4), in addition to the breaking of the conjugation between the benzene ring and the peptide bond. The 100° barrier in *o*-methoxy NMB appears to have the same origin. Two factors make the *o*-methoxy NMB 180° conformer significantly less favorable than the equilibrium one: (1) there is a very high repulsion between the oxygen atoms of the OCH_3 substituent and the C═O group (2.63 Å distance), and (2) the system loses the stabilizing hydrogen bond that exists in the equilibrium conformer (Figure 4).

Another feature of the NMB torsional potential is a low-lying transition state at 0° and 180° $C_a-C_a-C_c-N$ dihedral angles (Figure 5). This transition state was also observed for other computational levels by Vargas et al,[40] as well as for some other structurally similar molecules, such as benzamide.[42] It corresponds to a planar nitrogen atom with a 180° improper dihedral angle between C_c, N, H (of the NH group), and C_{methyl} atoms. Thus, the small (0.5 kcal/mol) barrier stems from the nitrogen atom going from the preferred pyramidal arrangement (accommodating a roughly tetrahedral configuration with the N lone pair) to the somewhat less favorable planar one. Consequently, the equilibrium NMB geometry has the $C_c-N-H_{NH}-C_{methyl}$ improper dihedral angle at ~162°.

The NMB torsional profile is remarkably similar to the one obtained for the C_a-N torsion in acetanilide (Figure 3a), which features a barrier of ~4 kcal/mol. The same can be said about the shape of the torsional potential of *o*-methoxy NMB in comparison to *o*-SCH_3 acetanilide (Figure 3b) but not about its barrier values. Upon addition of the *o*-SCH_3 group, the acetanilide barrier at 90° increases from ~4 to ~7 kcal/mol (the equivalent increase in going from NMB to *o*-methoxy NMB is from 4 to 5 kcal/mol). The 180° maximum in substituted acetanilide appears at >16 kcal/mol, twice the value of the equivalent barrier in *o*-methoxy NMB. This suggests an important conclusion: One can adjust flexibility or rigidity of the arylamide by simply exchanging S and O atoms in the substituent groups without altering other features such as charge or size of the side chains.[46]

III.B. Arylamide Chain Conformation in Aqueous Solution. To assess the influence of torsional barrier heights of backbone bonds on the overall shape of the arylamide compound, we performed MD simulations of **2** in aqueous solution using two sets of force field parameters (as described in the methods section), under otherwise identical conditions. Applying original GAFF torsional parameters is expected to significantly restrict the internal rotation around the bond of interest (CCCN torsional barrier ~29 kcal/mol). Inversely, we expect to see the molecule flexing primarily in the vicinity of the central benzene ring when we use torsional parameters derived from quantum mechanical studies of model compounds reported here and elsewhere.[10,11,15]

Indeed, MD simulation of the arylamide in solution using original GAFF shows that the $C_a-C_a-C_c-N$ dihedral angle is centered around 0° on both sides of the central benzene ring, with a narrow distribution (Figure 6a). This is a consequence of a very high (~29 kcal/mol) torsional barrier around this bond. Upon reducing the barrier to the value that corresponds to the particular chemical environment of the C_a-C_c bond in **2** (~9 kcal/mol), the distribution of the dihedral angle widens roughly by 30%, and is centered at ±25° (one side benzene ring at +26°, the other one at −23°). As will be discussed in section III.D, these conclusions are confirmed by results of REM simulations of arylamide in the presence of heparin.

The torsion around the C_a-N bond shows an opposite trend, due to the increase in internal rotation barrier height with respect to the original GAFF value (from ~2 kcal/mol for the original GAFF to ~16 kcal/mol in the modified GAFF). Whereas the dihedral angle distribution curves from original GAFF simulation are centered at ±130°, the modified GAFF ones are at ±175°. The modified GAFF $C_a-C_a-N-C_c$ dihedral angle distribution width does not differ much from the original GAFF case. A similar trend is observed in REM simulation of the arylamide in the presence of heparin when the original and the modified GAFF are compared (section III.D).

In summary, in the modified GAFF description, the side benzene rings and arginine chains rotate with respect to the central benzene ring mainly due to the more facile torsion around the C_a-C_c bond. The consequence of the two torsional

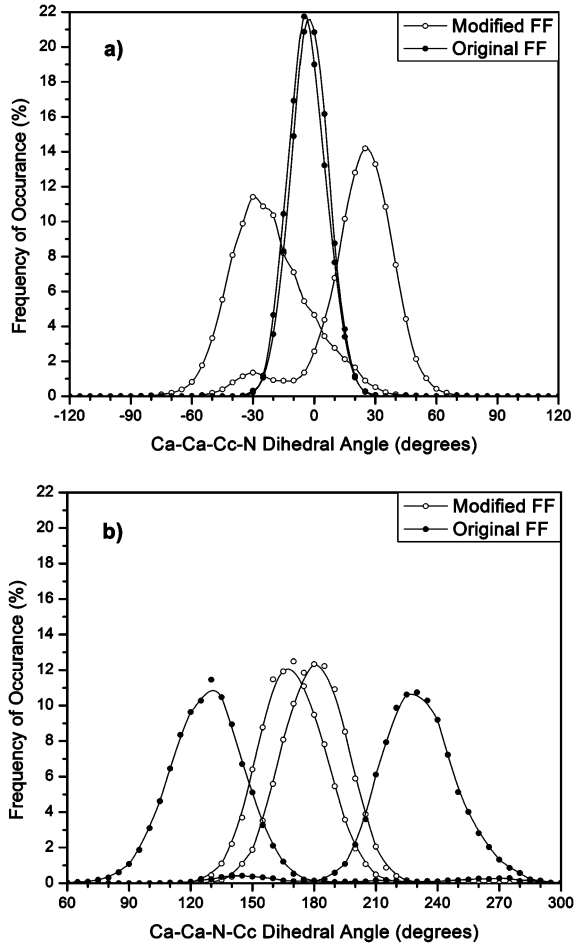

Figure 6. Dihedral angle distributions for key torsions in the arylamide, obtained from classical MD simulations using GAFF parameters modified to include the effect of the intramolecular environment (torsional parameters reported in this work and in refs 10 and 11) and original GAFF parameters: (a) $C_a-C_a-C_c-N$ dihedral angle distribution; (b) $C_a-C_a-N-C_c$ dihedral angle distribution. Note that there are two $C_a-C_a-C_c-N$ and two $C_a-C_a-N-C_c$ dihedral angles.

parameter changes being opposite (one increased, the other decreased), but with the C_a-C_c one much larger in absolute terms, is a net increase in flexibility of the arylamide backbone.

The influence that the modified torsional parameters have on the overall conformation of the arylamide can be seen in Figure 7. The molecule spends most of the simulation time in the configuration with the end-to-end distance (measured between guanidine carbon atoms of the two arginine chains) between 25 and 30 Å when modified GAFF is used, whereas that distance is between 20 and 26 Å when original GAFF parameters are used. Thus, the conformation resulting from the modified GAFF description yields a more extended shape than the one from the original GAFF.

III.C. Arylamide Chain Conformation in the Gas Phase. To assess the validity of the MD description of arylamide when torsional potentials discussed here are applied, we simulated a somewhat reduced form of **2** using AIMD. The advantage of AIMD is that the forces controlling the dynamics of the molecule are obtained from electronic structure calculations, performed simultaneously with the ionic dynamics, thus circumventing the use of predetermined, parametrized force fields. Due to the computational cost of AIMD, here we consider gas-phase dynamics of **3** (derived from **2** by removing parts of arginine chains to reduce the size of the system, see Figure 8a), thereby preserving the part of the structure important for

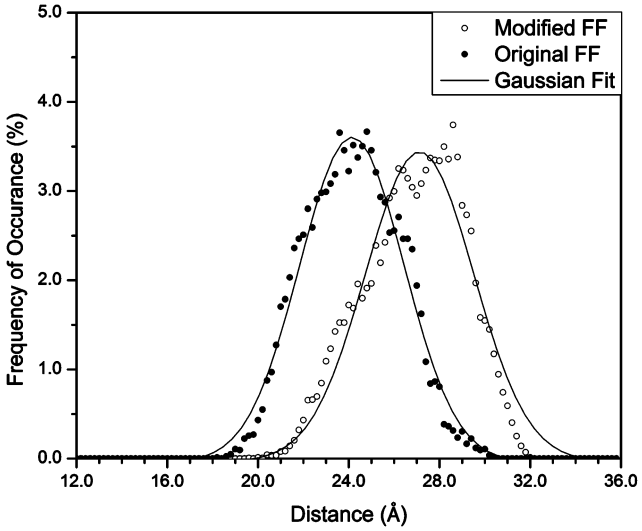

Figure 7. Distribution of the arylamide compound **2** end-to-end distance obtained from MD simulations using original GAFF and GAFF modified to include torsional parameters reported here and in refs 10 and 11. End-to-end distance is calculated as the distance between guanidine carbon atoms of the two arginine chains.

comparison with the results discussed in sections III.A and III.B. To remove the charges, **2** was further modified by replacing NH_3^+ groups by CH_3 groups. This alteration was necessary to allow backbone torsions to be controlled by torsional potentials of the C_a-C_c and C_a-N bonds, rather than to be governed by electrostatic interactions.

In analyzing the AIMD simulation, we focus on the $C_a-C_a-C_c-N$ and $C_a-C_a-N-C_c$ dihedral angles (parts a and b of Figure 8). The dihedral angle distribution curves obtained from a 9 ps AIMD run at 300 K are much closer to the modified GAFF ones than they are to the original GAFF one (parts c and d of Figure 8). The $C_a-C_a-C_c-N$ dihedral angle preference is at ~35°, significantly shifted from the original GAFF value of 0°. The AIMD and modified GAFF distribution curves for this dihedral angle are similarly broad, covering the same range of angle values, and thus display characteristics very unlike those of the original GAFF $C_a-C_a-C_c-N$ distribution curves (Figure 8c). The differences in the distribution features between the AIMD and modified GAFF results are attributed to the disparity in the sampling time between the two techniques (AIMD and MD), as well as the fact that the simulated structures are not the same. The $C_a-C_a-N-C_c$ dihedral angle distribution closely resembles the modified GAFF behavior and is clearly different from that predicted by the original GAFF (Figure 8d). Thus, AIMD independently confirms our observations obtained by modified GAFF MD simulations. We conclude that model compounds NMB, *o*-methoxy NMB, acetanilide, and *o*-thiomethyl acetanilide are sufficiently large to encompass important arylamide features and serve as model compounds; that is, torsional parameters derived from these models properly describe the intramolecular environment of the arylamide and its influence on the flexibility of the backbone.

We also note that we observe a tilting of $SCH_2CH_2CH_3$ groups out of the benzene ring plane (Figure 8b), as predicted by Doerksen's work on model compounds comprising one benzene ring.[10] This observation validates the need for an implementation of the $C_a-C_a-S-C_{methyl}$ torsional parameter, obtained from quantum chemical calculations on *o*-thiomethyl acetanilide.[10] An accurate description of the degree of torsional freedom of thioether and ether substituents is important in this case, because of the fact that charged NH_3^+ groups responsible

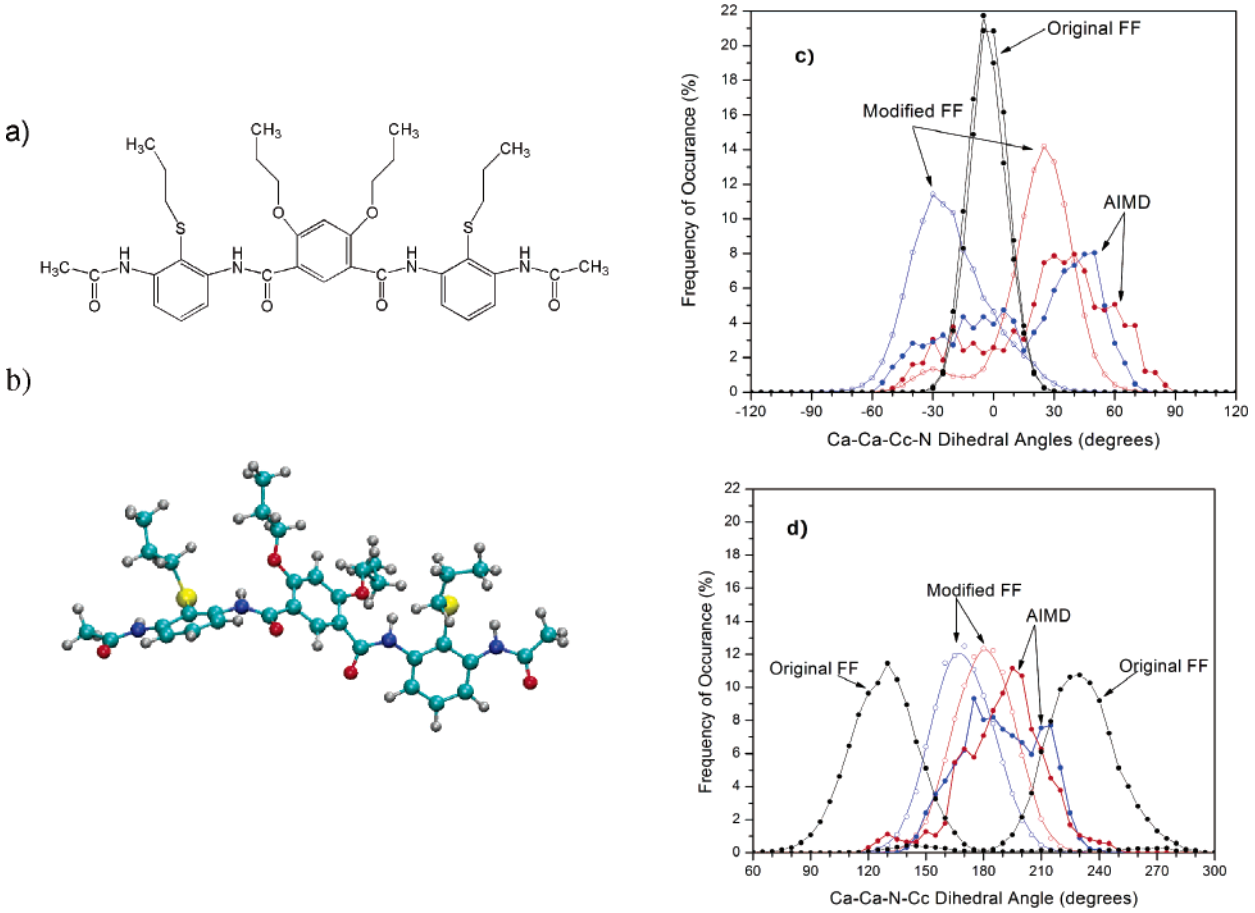

Figure 8. (a) Structure of a reduced arylamide model used in AIMD simulations. It is derived from compound **2** by removing the terminal (arginine) $CH_2CH_2NHCNHNH_2^+$ chains and by substituting all NH_3^+ groups by CH_3 groups. (b) Snapshot from the AIMD simulation of the reduced arylamide model illustrating backbone bending as a consequence of primarily the C_a-C_c torsion, as well as $SCH_2CH_2CH_3$ chain tilting out of the benzene ring planes: carbon, blue; oxygen, red; nitrogen, dark blue; hydrogen, silver; sulfur, yellow. (c) $C_a-C_a-C_c-N$ and (d) $C_a-C_a-N-C_c$ dihedral angle distribution curves from the AIMD (9 ps) and modified GAFF MD (3 ns) simulations. Original GAFF MD curves are given for comparison. Note that there are two $C_a-C_a-C_c-N$ and two $C_a-C_a-N-C_c$ dihedral angles. For clarity, one of the symmetrical dihedral angles is given in blue, the other one in red color, for both the AIMD and modified GAFF MD distributions. Original GAFF MD curves are given in black.

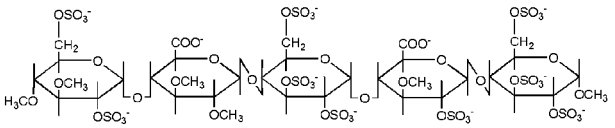

Figure 9. Chemical structure of the pentasaccharide sequence of heparin used in this study. This sequence is responsible for the binding of heparin to antithrombin III (causing hemorrhage in up to 30% of heparin treatment cases)[47] and thus is the key section of heparin molecule that should react with the antidote.

for arylamide binding to heparin terminate four such substituents. Consequently, their location in the complex with heparin depends on the torsional motion (and torsional potential) around the bonds in the side chains.

III.D. Arylamide Chain Conformation in Aqueous Solution in the Presence of Heparin. We now look at how the increased flexibility of arylamide affects its interaction with heparin, which we take as an example of the biochemical target of arylamide polymers (Figure 9). Heparin is known as a biological macromolecule with the highest negative charge density. Therefore, arylamide and heparin are expected to interact primarily through electrostatic interaction between the positively charged groups of heparin and negatively charged side chains of the arylamide. We present results of REM and conventional MD simulations of the arylamide/heparin system in aqueous solution using both the force field with the high barrier for torsion around the C_a-C_c bond, and the low barrier for the torsion around the C_a-N bond, and the force field in which we implement the barriers discussed in section III.A and obtained by Doerksen et al.[10,11]

The relevant dihedral angle distributions (parts a and b of Figure 10) obtained from both the conventional and REM simulations are quite different for original and modified force fields. Thus, $C_a-C_a-C_c-N$ distribution stemming from the modified GAFF is centered at $\pm 30°$, similar to the result obtained from the arylamide alone (conventional MD, Figure 6), and is very different from the distribution obtained by the REM simulation using the original GAFF, which is centered at 0° (same as in the case of arylamide alone, Figure 6). The same is true for the $C_a-C_a-N-C_c$ angle for which the supporting conclusions were derived in section III.B.

The degree of flexibility observed in the MD simulation with the torsional parameters obtained from quantum chemical calculations is evidently higher. What is important, however, is the impact of this flexibility on the description of binding interaction between heparin and arylamide. Starting from the same initial relative configurations, the relative positions of arylamide and heparin after several nanoseconds of conventional MD simulation are quite different for the two cases. The less flexible form interacts with only a few charged heparin OSO_3^- groups and does not involve all of its charged side chains in the interaction (Figure 11a). The more flexible form, however, relaxes in such a way as to accommodate a significantly larger

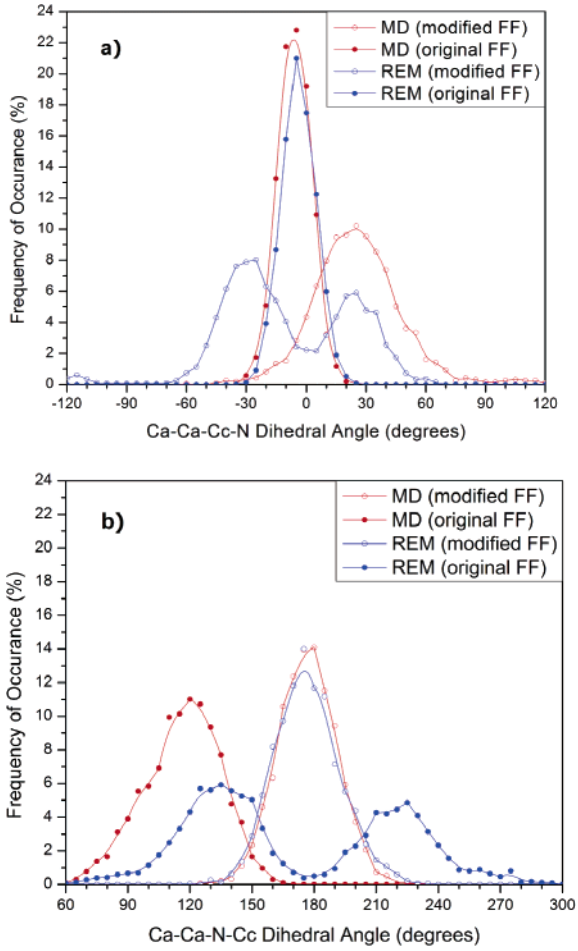

Figure 10. Dihedral angle distributions for key torsions in the arylamide in the presence of heparin, obtained from REM (blue) and conventional MD (red) simulations using GAFF parameters modified to include the effect of the intramolecular environment (open circles) and original GAFF (full circles) parameters: (a) $C_a-C_a-C_c-N$ dihedral angle distribution; (b) $C_a-C_a-N-C_c$ dihedral angle distribution. Note that there are two $C_a-C_a-C_c-N$ and two $C_a-C_a-N-C_c$ dihedral angles but, for clarity, only one of the equivalent angles is plotted.

number of electrostatic and hydrogen-bonding contacts, thus leading to more effective binding. In the case of the high C_a-C_c torsional parameter, only one side of arylamide takes part in binding; when this parameter is reduced, arylamide lines up with heparin and, more importantly, allows more of its side groups to interact by increasing the freedom of rotation around the backbone bonds (parts a and b of Figure 11).

The effect can be quantified by counting the contacts made between the charged groups of the two species. We apply the following distance dependent criteria for the counting: a value of 1.5 is assigned to the counting function if N atoms of the NH_3^+ or guanidine groups[48] in the arylamide are closer than 4 Å to the S atoms of the SO_3^- groups or C atoms of the COO^- groups of heparin. Values of 1.0, 0.5, and 0.0 are assigned when these distances fall in intervals of 4−5, 5−6, and >6 Å, respectively. Figure 12 (corresponding to the last 3 ns of the conventional MD simulation and 4 ns of REM simulation at 300 K) shows that there is a significant (∼20%) increase in the number of contacts between the charged groups of the two species when torsional parameters reflecting a specific intramolecular environment of the bonds undergoing internal rotation are applied. One should note that such an increase, resulting in the number of contacts being between 12 and 17 most often, for the molecules that have a total of 8 and 11 charged groups

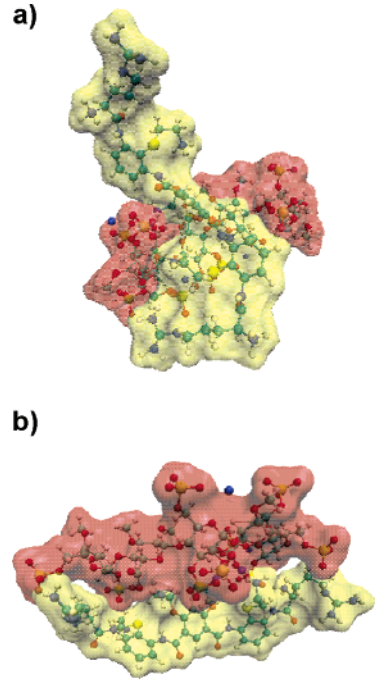

Figure 11. Snapshots from the MD trajectories of arylamide/heparin complex, illustrating differences in binding mode between the simulations based on original (a) and modified (b) GAFF parameters: arylamide, yellow surface; heparin, red surface.

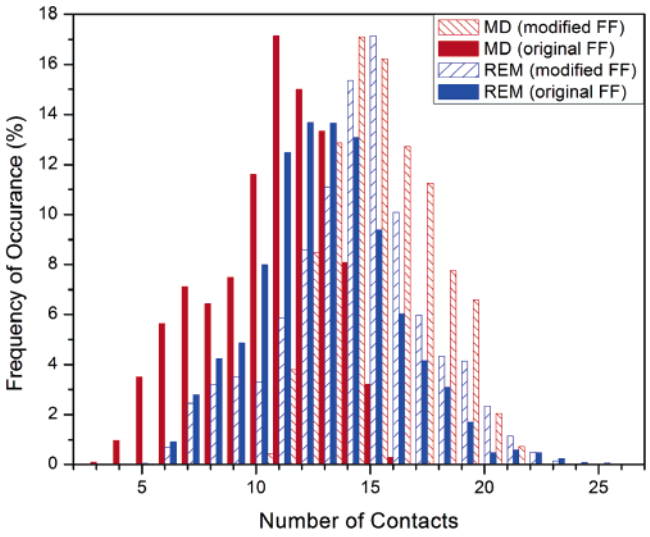

Figure 12. Distribution of the number of contacts between the charged groups of arylamide and heparin, obtained from REM simulation (blue), for both the modified and original GAFF (see legend). For comparison, results of the conventional MD run (last 3 ns) are also given, in red. The number of contacts is calculated as follows: a value of 1.5 is assigned to the counting function if N atoms of the NH_3^+ or guanidine groups[48] in the arylamide are closer than 4 Å to the S atoms of the SO_3^- groups or C atoms of the COO^- groups of heparin. Values of 1.0, 0.5, and 0.0 are assigned when these distances fall in intervals of 4−5, 5−6, and >6 Å, respectively. A bin size of 1 contact unit was used in formation of the histogram; thus, a bar at N number of contacts includes all the conformations that fall in the range $N \leq$ number of contacts $< N + 1$, N being an integer.

leads to practically a maximal binding mode. This is illustrated by a snapshot from the simulation (using modified GAFF parameters, Figure 13), where we observe that besides the traditional electrostatic interactions, SO_3^- and COO^- groups on one hand and NH_3^+ and guanidine groups on the other hand are positioned in an optimal manner for a number of hydrogen

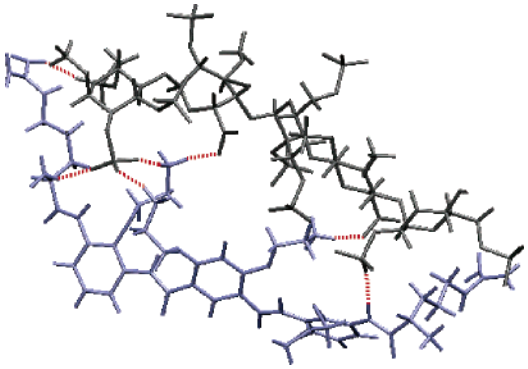

Figure 13. Snapshot from the arylamide/heparin trajectory (obtained using modified GAFF, conventional MD), showing a number of hydrogen bonds (red) between heparin (gray) and arylamide (blue), strengthening the interaction between the species. The criteria used for hydrogen bond determination were a distance cutoff of 3.2 Å and an angle cutoff of 30°.

bonds to be formed. Thus, accounting for the specific intramolecular environment and interactions such as hydrogen-bonding in the MD simulation parameters leads to a tighter binding description.

IV. Discussion

There are two related aspects to the analysis of our results. The first one comes from comparison between original GAFF and modified GAFF descriptions, which tells us how sensitive the biochemical function of arylamide binding to heparin is to the torsional potentials applied in the simulation. The other aspect deals with how detailed and accurate information on torsional potentials obtained from quantum chemical calculations on representative model compounds can be used to control the arylamide biochemical function and help in designing optimal arylamide forms.

By modifying GAFF to include the quantum mechanically obtained barriers on model compounds that encompass specific intramolecular environments of the bonds undergoing torsion (such as hydrogen-bonding groups), we effectively reduce the barrier around the C_a-C_c bond and increase the barrier around the C_a-N bond. The barrier change is much more pronounced for the C_a-C_c bond than for the C_a-N bond, and we therefore see a more flexible arylamide backbone than when using the original GAFF force field. The MD description of the arylamide binding to heparin is very sensitive to the torsional parameters used in the simulation: Changing the torsional parameters alone leads to a mechanism that explains and relates to experimental results much better than when generalized (unmodified) parameters are used. For example, our REM simulation with the original GAFF implies that the complex between arylamide and heparin usually has 10−15 contacts between the charged groups and that the interaction sites are concentrated in only one part of the arylamide (Figures 11 and 12). This leads to a (erroneous) conclusion that the design efforts should go in a direction of spatially concentrating charged groups in arylamide. On the contrary, the modified force field shows why this form of arylamide, as opposed to the other ones experimentally tested for their antidote activity,[7] has the optimal structure for binding with heparin: on the average, the majority of the charged groups are involved in binding, and many of the groups make multiple contacts with the heparin groups (12−17 contacts, Figure 12). Therefore, we can use torsional parameters as a tool for adjusting or improving certain functional features of arylamides.

Knowing torsional potentials for a series of bonds in a series of intramolecular environments allows us to achieve a significant level of control by modifying features of the side chains or bonds that undergo torsion. For example, including ortho substituents which have O or S atoms linking to the benzene rings leads the molecule from almost free rotation around the backbone bonds (excluding amide bonds) to significantly restricted rotation (e.g., torsional barriers go from ∼4 to ∼9 or ∼16 kcal/mol). Two main attributes influence these changes: the nature of the bond undergoing rotation (i.e., C_a-C_c vs C_a-N) and the size and hydrogen-bonding ability of the atom (in our case S vs O) in the substituent closest to the bond undergoing torsion. Once a mechanism of biochemical function, in this case binding of arylamide to heparin, is analyzed, one can fine-tune the conformation of the molecule by such substitutions with a goal of increasing the effectiveness and specificity of the function.

V. Conclusions

By combining three computational chemistry techniques, we arrive at several conclusions related to conformation of arylamides and their binding to one of the arylamide biochemical targets, heparin. We have shown that there is a significant degree of sensitivity of arylamide conformation and heparin binding mechanism on details of its structure that influence torsional potentials for bonds composing the backbone. Thus, an accurate account (in terms of torsional parameters used in force fields) of the intramolecular environment, including hydrogen-bonding and steric effects, is critical for obtaining insight into the relationship between arylamide structure and function. This is achieved by applying quantum chemically derived torsional potentials from compounds that mimic essential structural features of the polymer. Our AIMD simulations indicate that essential torsional features of **2** are taken into account by applying torsional parameters based on *o*-thiomethyl acetanilide and *o*-methoxy *N*-methylbenzamide. We find that the presence of an ortho ether or thioether substituent on the benzene rings in the arylamide backbone affects torsional potentials and, consequently, the backbone flexibility in a similar fashion but to different extents. The differences in torsional potential energy profiles between *o*-thiomethyl acetanilide and *o*-methoxy *N*-methylbenzamide stem from different bonds undergoing rotation, as well as the different chemical nature of the atoms connecting the substituents to the benzene rings. Thus, subtle changes in chemical structure, such as the choice of using thioether, ether, or aliphatic side chains, can yield different binding modes and consequently can potentially be used as a tool for influencing potency and specificity of arylamides as biomedical agents.

Acknowledgment. This research was supported in part by the National Institutes of Health (Grant No. EB002048) and the National Science Foundation. Computer time from Pittsburgh Supercomputing Center, under the aegis of NRAC, is greatly appreciated. Z.L. and V.P. acknowledge support from the H. O. West Foundation and NSF (Grant No. CHE-0420556). I.I. acknowledges financial support from the Burroughs Wellcome Fund through a La Jolla Interfaces in Science interdisciplinary fellowship. NWChem version 4.5, as developed and distributed by Pacific Northwest National Laboratory, P.O. Box 999, Richland, WA 99352, and funded by the U.S. Department of Energy, was used to obtain some of these results. NAMD was developed by the Theoretical and Computational Biophysics Group in the Beckman Institute for Advanced Science and Technology at the University of Illinois at Urbana-Champaign.

Supporting Information Available: Energies and $C_a-C_a-C_c-N$ dihedral angles of NMB and *o*-methoxy NMB conformers

at various computational levels. This material is available free of charge via the Internet at http://pubs.acs.org.

References and Notes

(1) Gellman, S. H. *Acc. Chem. Res.* **1998**, *31*, 173−180.

(2) Tew, G. N.; Liu, D. H.; Chen, B.; Doerksen, R. J.; Kaplan, J.; Carroll, P. J.; Klein, M. L.; DeGrado, W. F. *Proc. Natl. Acad. Sci. U.S.A.* **2002**, *99*, 5110−5114.

(3) Liu, D. H.; Choi, S.; Chen, B.; Doerksen, R. J.; Clements, D. J.; Winkler, J. D.; Klein, M. L.; DeGrado, W. F. *Angew. Chem., Int. Ed.* **2004**, *43*, 1158−1162.

(4) Porter, E. A.; Wang, X.; Lee, H. S.; Weisblum, B.; Gellman, S. H. *Nature* **2000**, *405*, 298−298.

(5) Porter, E. A.; Wang, X. F.; Lee, H. S.; Weisblum, B.; Gellman, S. H. *Nature* **2000**, *404*, 565−565.

(6) Zasloff, M. *Nature* **2002**, *415*, 389−395.

(7) Choi, S.; Clementi, D.; Pophristic, V.; Ivanov, I.; Vemparala, S.; Klein, M. L.; DeGrado, W. F. *Angew. Chem., Int. Ed.* **2005**, *41*, 6599.

(8) Kriek, E.; Miller, J. A.; Juhl, U.; Miller, E. C. *Biochemistry* **1967**, *6*, 177.

(9) Topper, R. Q.; Chung, K.; Boelke, C. M.; Louie, D.; Kang, J. S.; Hannan, R.; Kiang, T.; Chan, L. H. *Theor. Chem. Acc.* **2003**, *109*, 233−238.

(10) Doerksen, R. J.; Chen, B.; Liu, D. H.; Tew, G. N.; DeGrado, W. F.; Klein, M. L. *Chem.—Eur. J.* **2004**, *10*, 5008−5016.

(11) Doerksen, R. J.; Chen, B.; Klein, M. L. *Chem. Phys. Lett.* **2003**, *380*, 150−157.

(12) Vinogradov, S. A. *Org. Lett.* **2005**, *7*, 1761−1764.

(13) Berl, V.; Schmutz, M.; Krische, M. J.; Khoury, R. G.; Lehn, J. M. *Chem.—Eur. J.* **2002**, *8*, 1227−1244.

(14) Shih, N. Y.; Albanese, M.; Anthes, J. C.; Carruthers, N. I.; Grice, C. A.; Lin, L.; Mangiaracina, P.; Reichard, G. A.; Schwerdt, J.; Seidl, V.; Wong, S. C.; Piwinski, J. J. *Bioorg. Med. Chem. Lett.* **2002**, *12*, 141−145.

(15) Detailed results from similar studies on other model compounds will be reported elsewhere. See also Vemparala, S.; Ivanov, I.; Pophristic, V.; Spiegel, K.; Klein, M. L. *J. Comput. Chem.* **2006**, *27*, 693−700.

(16) Frisch, M. J.; Trucks, G. W.; Schlegel, H. B.; Scuseria, G. E.; Robb, M. A.; Cheeseman, J. R.; Montgomery, J. A., Jr.; Vreven, T.; Kudin, K. N.; Burant, J. C.; Millam, J. M.; Iyengar, S. S.; Tomasi, J.; Barone, V.; Mennucci, B.; Cossi, M.; Scalmani, G.; Rega, N.; Petersson, G. A.; Nakatsuji, H.; Hada, M.; Ehara, M.; Toyota, K.; Fukuda, R.; Hasegawa, J.; Ishida, M.; Nakajima, T.; Honda, Y.; Kitao, O.; Nakai, H.; Klene, M.; Li, X.; Knox, J. E.; Hratchian, H. P.; Cross, J. B.; Bakken, V.; Adamo, C.; Jaramillo, J.; Gomperts, R.; Stratmann, R. E.; Yazyev, O.; Austin, A. J.; Cammi, R.; Pomelli, C.; Ochterski, J. W.; Ayala, P. Y.; Morokuma, K.; Voth, G. A.; Salvador, P.; Dannenberg, J. J.; Zakrzewski, V. G.; Dapprich, S.; Daniels, A. D.; Strain, M. C.; Farkas, O.; Malick, D. K.; Rabuck, A. D.; Raghavachari, K.; Foresman, J. B.; Ortiz, J. V.; Cui, Q.; Baboul, A. G.; Clifford, S.; Cioslowski, J.; Stefanov, B. B.; Liu, G.; Liashenko, A.; Piskorz, P.; Komaromi, I.; Martin, R. L.; Fox, D. J.; Keith, T.; Al-Laham, M. A.; Peng, C. Y.; Nanayakkara, A.; Challacombe, M.; Gill, P. M. W.; Johnson, B.; Chen, W.; Wong, M. W.; Gonzalez, C.; Pople, J. A. *Gaussian 03*; Gaussian, Inc.: Wallingford, CT, 2004.

(17) High Performance Computational Chemistry Group. *NWChem, A Computational Chemistry Package for Parallel Computers*, version 4.5; Pacific Northwest National Laboratory: Richland, WA, 2003.

(18) Kendall, R. A.; Aprà, E.; Bernholdt, D. E.; Bylaska, E. J.; Dupuis, M.; Fann, G. I.; Harrison, R. J.; Ju, J.; Nichols, J. A.; Nieplocha, J.; Straatsma, T. P.; Windus, T. L.; Wong, A. T. *Comput. Phys. Commun.* **2000**, *128*, 260−283.

(19) Car, R.; Parrinello, M. *Phys. Rev. Lett.* **1985**, *55*, 2471−2474.

(20) *CPMD*. Copyright IBM Corp. 1990−2001. Copyright Max-Planck-Institute für Festkörperforschung Stuttgart, 1997−2004.

(21) Hamprecht, F. A.; Cohen, A. J.; Tozer, D. J.; Handy, N. C. *J. Chem. Phys.* **1998**, *109*, 6264−6271.

(22) Vanderbilt, D. *Phys. Rev. B* **1990**, *41*, 7892−7895.

(23) Laasonen, K.; Pasquarello, A.; Car, R.; Lee, C.; Vanderblit, D. *Phys. Rev. B* **1993**, *47*, 10142−10153.

(24) Martyna, G. J.; Klein, M. L.; Tuckerman, M. *J. Chem. Phys.* **1992**, *97*, 2635−2643.

(25) Nose, S. *Mol. Phys.* **1984**, *52*, 255−268.

(26) Hoover, W. G. *Phys. Rev. A* **1985**, *31*, 1695−1697.

(27) Nose, S. *J. Chem. Phys.* **1984**, *81*, 511−519.

(28) Wang, J.; Wolf, R. M.; Caldwell, J. W.; Kollman, P. A.; Case, D. A. *J. Comput. Chem.* **2004**, *25*, 1157−1174.

(29) Jakalian, A.; Jack, D. B.; Bayly, C. I. *J. Comput. Chem.* **2002**, *23*, 1623−1641.

(30) Jakalian, A.; Bush, B. L.; Jack, D. B.; Bayly, C. I. *J. Comput. Chem.* **2000**, *21*, 132−146.

(31) Woods, R. J.; Dwek, R. A.; Edge, C. J.; Fraserreid, B. *J. Phys. Chem.* **1995**, *99*, 3832−3846.

(32) Wang, J. M.; Cieplak, P.; Kollman, P. A. *J. Comput. Chem.* **2000**, *21*, 1049−1074.

(33) Cornell, W. D.; Cieplak, P.; Bayly, C. I.; Gould, I. R.; Merz, K. M.; Ferguson, D. M.; Spellmeyer, D. C.; Fox, T.; Caldwell, J. W.; Kollman, P. A. *J. Am. Chem. Soc.* **1995**, *117*, 5179−5197.

(34) Huige, C. J. M.; Altona, C. *J. Comput. Chem.* **1995**, *16*, 56−79.

(35) Jorgensen, W. L.; Chandrasekhar, J.; Madura, J. D.; Impey, R. W.; Klein, M. L. *J. Chem. Phys.* **1983**, *79*, 926−935.

(36) Mitsutake, A.; Sugita, Y.; Okamoto, Y. *Biopolymers* **2001**, *60*, 96−123.

(37) Kale, L.; Skeel, R.; Bhandarkar, M.; Brunner, R.; Gursoy, A.; Krawetz, N.; Phillips, J.; Shinozaki, A.; Varadarajan, K.; Schulten, K. *J. Comput. Phys.* **1999**, *151*, 283−312.

(38) Case, D. A.; Darden, T. A.; Cheatham, T. E., III; Simmerling, C. L.; Wang, J.; Duke, R. E.; Luo, R.; Merz, K. M.; Wang, B.; Pearlman, D. A.; Crowley, M.; Brozell, S.; Tsui, V.; Gohlke, H.; Mongan, J.; Hornak, V.; Cui, G.; Beroza, P.; Schafmeister, C.; Caldwell, J. W.; Ross, W. S.; Kollman, P. A. *AMBER 8*; University of California: San Francisco, CA, 2004.

(39) Hummel, J. P.; Flory, P. J. *Macromolecules* **1980**, *13*, 479−484.

(40) Vargas, R.; Garza, J.; Dixon, D.; Hay, B. P. *J. Phys. Chem. A* **2001**, *105*, 774−778.

(41) Allen, F. H.; Bellard, S.; Brice, M. D.; Cartwright, B. A.; Doubleday, A.; Higgs, H.; Hummelink, T.; Hummelinkpeters, B. G.; Kennard, O.; Motherwell, W. D. S.; Rodgers, J. R.; Watson, D. G. *Acta Crystallogr., Sect. B* **1979**, *35*, 2331−2339.

(42) Campomanes, P.; Menendez, M. I.; Sordo, T. L. *J. Phys. Chem. A* **2002**, *106*, 2623−2628.

(43) Acetanilide models internal rotation around the C_a−N bond. The two substituted compounds (*o*-OCH_3 and *o*-SCH_3 acetanilide) capture the essential environment of the bond undergoing torsion, present in arylamides with applications we are interested in.

(44) Our BLYP results are within 0.15 kcal/mol of Vargas et al. BLYP value; the MP2 values are, however, 0.6−1.0 kcal/mol higher than Vargas' MP2/DZP value.

(45) Durig, J. R.; Bist, H. D.; Furic, K.; Qiu, J.; Little, T. S. *J. Mol. Struct.* **1985**, *129*, 45−56.

(46) Present results suggest that the addition of the SCH_3 group as opposed to OCH_3 in the ortho position rigidizes the molecule much more efficiently. However, in comparing NMB and acetanilide, one should note that there are two main differences between the systems: in NMB, we look at the rotation around the C_a−C_c bond; in acetanilide, the rotation occurs around the C_a−N bond. Also, the ortho substituent in *o*-methoxy NMB is an ether group, whereas it is a thioether group in substituted acetanilide. Direct comparison of analogous compounds is beyond the scope of this article and will be addressed in a future publication.

(47) Capila, I.; Linhardt, R. J. *Angew. Chem., Int. Ed.* **2002**, *41*, 391−412.

(48) Only the terminal, primary N atoms of the guanidine group were used. The secondary N atom (connecting the guanidine group to the rest of arginine and arylamide) was not used.